CHAPTER 2

Transformation of nonbreaking waves over a bar

S. Beji[1], T. Ohyama[2], J.A. Battjes[3] and K. Nadaoka[4]

Abstract

Data collected from measurements performed in waves propagating over a trapezoidal bar on a horizontal bottom are used to test a fully nonlinear numerical model. The experiments include both regular and random waves. Wave form evolutions in the shoaling region, the near resonant wave-wave interactions over the bar, and finally the decomposition behind the bar are well predicted. The results provide assurance for the reliability of the numerical model.

1. Introduction

Numerical modeling of evolving surface gravity waves based on the full nonlinear equations for irrotational motion was initiated by Longuet-Higgins and Cokelet (1976). Numerous alternative models have been presented since (Vinjé and Brevig, 1981; Dold and Peregrine, 1984). Surface profiles predicted by these models are in general quite realistic, even in the phases of profile steepening and turnover as in plunging breakers

---

[1]Former post-doctorate fellow at Delft University of Technology. Present employment: Naval Architecture and Ocean Engineering Faculty, Istanbul Technical University, Turkey.

[2]Research scientist, Env. Eng. Div., Shimizu Corp., Etchujima 3-4-17, Koto-ku, Tokyo 135, Japan.

[3]Professor, Dept. of Civil Eng., Delft University of Technology, P.O. Box 5048, 2600 GA Delft, The Netherlands.

[4]Assoc. Prof., Dept. of Civil Eng., Tokyo Institute of Tech., O-okayama, Meguro-ku, Tokyo 152, Japan.

(prior to impact). However, quantitative comparisons between predictions and observations are rarely given. The purpose of the present paper is to give such comparisons, for the demanding case of deformation and decomposition of near-breaking waves passing over a shallow bar.

It is known that relatively long waves passing over a bar or another submerged obstacle decompose into shorter components. In the shoaling region the amplitudes of the bound harmonics are initially relatively small. If the wave field continues to propagate into a shallower region, such that the medium becomes non-dispersive for this particular wave field, then the near resonance conditions for triplet-interactions are satisfied (Phillips, 1960). At this stage, a rapid energy flow from the primary wave components to the higher harmonics is observed and the amplitudes of higher harmonic components become appreciable.

The passage into deeper water results in the release of the bound harmonics followed by interactions taking place among these released wave components, which introduces drastic and rapid changes in wave forms. During this final stage, the amplitude of higher harmonics become comparable with, in some cases larger than, the primary wave amplitudes (Kojima, H. *et al.*, 1990; Ohyama and Nadaoka, 1991; Beji and Battjes, 1992). Obviously, predicting the evolutions of a given incident wave field in such regions poses a real challenge; this suggests a good test case for a nonlinear numerical wave propagation model.

The paper presents a brief account of a comparison of results of simulations with a numerical nonlinear model with experimental data for conditions as described above. For details, reference is made to Ohyama et al. (1992).

2. Experiments

The measurements reported here were carried out as a subset of a larger program, an account of which can be found in Beji and Battjes (1992).

The experiments were performed in a wave flume of the Department of Civil Engineering, Delft University of Technology. The flume is 37.7 m long, 0.8 m wide, and 0.75 m high. It is equipped with a hydraulically driven, piston-type random-wave generator. The bottom profile is sketched in Figure 1.

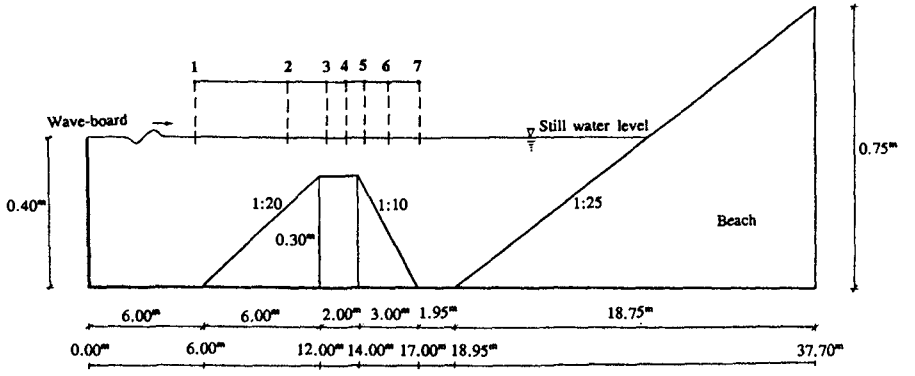

Figure 1. Definition sketch of wave flume and locations of wave gages.

A submerged trapezoidal bar with an upslope of 1:20 and a 2 m horizontal crest followed by a 1:10 downslope was constructed. The still water depth was 0.4 m in the deeper region and 0.1 m in the shallowest part above the horizontal section. At the end of the flume opposite to the wave generator, a roughened plane beach with a 1:25 slope served as a wave absorber.

Measurements of the free surface displacements were made with parallel-wire resistance gages at 7 different locations as shown in Figure 1. The time history of the wave-board displacement was recorded also. In each run, data were recorded simultaneously from 8 separate channels at a sampling frequency of approximately 25 Hz.

Four different measurements were realized: two different spectral shapes (periodic waves with a spike spectrum and random waves with a JONSWAP target spectrum), and two different peak frequencies (0.5 Hz and 0.8 Hz, referred to as the "long" waves and the "short" waves, respectively). All the measurements reported here were for non-breaking waves. The following incident wave heights were selected for regular waves: 2.0 cm for 0.5 Hz, and 2.5 cm for 0.8 Hz. Irregular waves required somewhat smaller incident significant wave heights to prevent occasional breaking. Thus, for irregular waves the following incident significant waves heights ($H_{1/3}$) were used: 1.8 cm for 0.5 Hz, and 2.3 cm for 0.8 Hz.

3. Numerical model

Computations have been carried out with a numerical model developed by Ohyama and Nadaoka (1991). It is based on the time-dependent boundary element method for potential flow. The field equations outside the sponge layer at the downwave side (Bernoulli and Laplace) and the boundary conditions at the bottom and the free surface are standard and are not reproduced here.

Figure 2 is an illustration of the numerical "wave tank", specifying the geometry and the labelling of the contour around the computational domain.

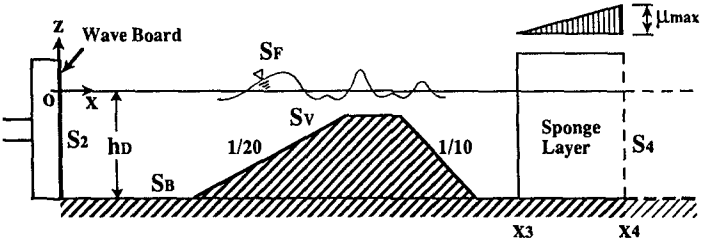

Figure 2. Computational domain.

The original version of the model contains a non-reflective wave generator, which combines a vertically distributed wave-making source with a numerical filter. However, in the present calculations the same wave generating method (piston-type) is used as in the model experiments, as expressed by the following equation:

$$\frac{\partial \phi}{\partial x} = U(t) \qquad (on\ S_2), \qquad (1)$$

in which ϕ is the velocity potential and U is the horizontal velocity of the wave board.

A numerical wave-absorption filter is located at the trailing end of the domain for the open boundary treatment. The filter is composed of a sponge layer, which absorbs the incoming wave energy by frictional damping according to the following equation:

$$\frac{\partial \phi}{\partial x} = -\frac{1}{\sqrt{gh_D}} \left(\frac{\partial \phi}{\partial t} + \mu\phi - \int_{x_3}^{x_4} \frac{\partial \mu}{\partial x} \phi |_{on\ S_F} dx \right) \qquad (on\ S_4), \quad (3)$$

in which μ is the damping factor of the sponge layer, of which the magnitude is distributed linearly in the layer, as shown in Figure 2, in order to reduce the wave reflection at the leading side of the layer. In view of the results of a previous study (Ohyama and Nadaoka, 1991), the width of the sponge layer is set nearly equal to the incident wave length (corresponding to the peak frequency in case of random waves), and the maximum value of the damping factor in the sponge layers, μ_{max}, is given as $\mu_{max}(h_D/g)^{1/2}=0.25$. At the leeside of the sponge layer, a Sommerfeld type radiation condition was applied to absorb whatever wave energy would be left after passing through the sponge layer.

Applying Green's theorem and the weighted residual method to the governing equations, integral equations can be derived; these are discretized spatially by using linear elements. In the discretized equations, ϕ (on S_F, S_V, S_2 and S_4), and $\partial\phi/\partial t$, η and $\partial\eta/\partial t$ (on S_F) are invoked as unknown variables. These variables are rewritten by using $\Delta\phi$ and $\Delta\eta$ which are the increments of ϕ and η, respectively, during the time increment Δt. Linear algebraic equations to be solved for $\Delta\phi$ (on S_F, S_V, S_2, and S_4) and $\Delta\eta$ (on S_F) are consequently obtained.

In all the computations examined, the time increment, Δt, was set to 1/32 of the incident wave period (spectral peak period for random waves). The horizontal projection of the distance between the surface nodes, Δx, on the other hand, was varied in space. The values relative to the incident wave lengths, $\Delta x/L$, were 1/15 for the interval $0 \le x \le 7.6$m and 1/40 for $x > 7.6$m for the 0.5-Hz waves, and were 1/15 for $0 \le x \le 10.0$m and 1/20 for $x > 10$m for the 0.8 Hz-waves.

The only experimental data used as input to the numerical model are the bottom profile, the still-water level, and the time history of the wave-board displacement (used to calculate the wave-board velocity U(t) in eq. 1); on the downwave side, full absorption has been assumed. The initial condition for each case was the still-water condition, i.e., $\phi=\eta=0$. Numerical results after 10 periods from the cold start are used for the subsequent discussion.

4. Comparisons of measurements and computations

For the case of the long (f = 0.5 Hz), monochromatic waves, Figures 3a-3d show the comparisons of measured and computed wave profiles at the stations 1,3,5,7, and Figure 4 shows the spatial evolutions of the lowest three harmonics amplitudes of the surface displacement. The elevations have been normalized with H_0, the target value of the incident wave height.

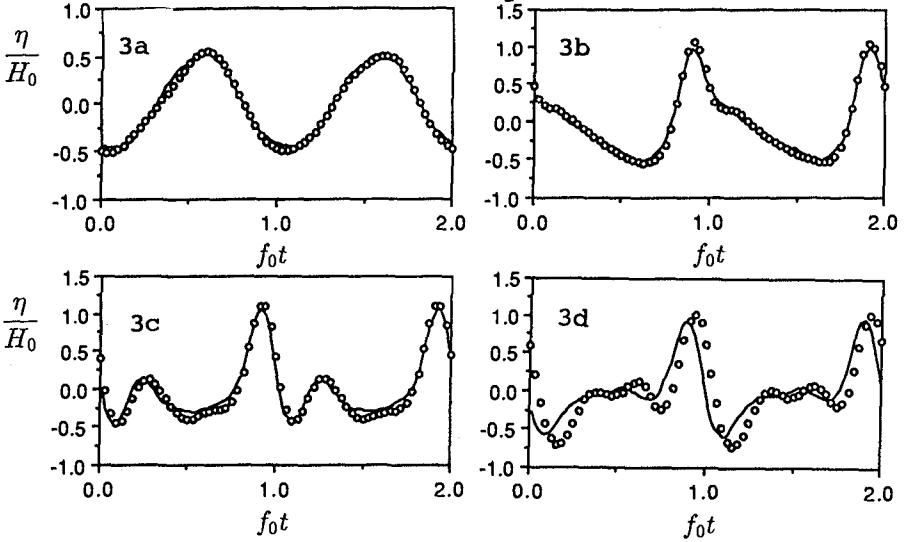

Figure 3. Measured (—) and computed (ooo) wave profiles for monochromatic waves, f=0.5 Hz, at stations 1,3,5 and 7 (a,b,c and d).

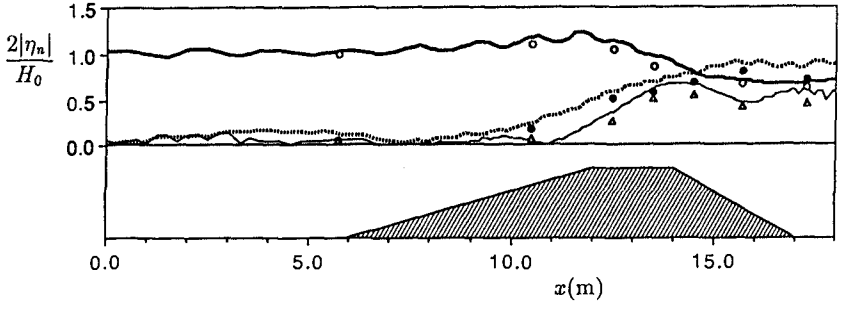

Figure 4. Measured (o: n=1)(•: n=2)(Δ: n=3) and computed (▬: n=1)(„„: n=2)(—: n=3) spatial evolution of harmonic amplitudes for monochromatic waves, f=0.5 Hz.

The overall agreement is excellent, especially in the upslope region and over the horizontal part. In the downslope region, some minor differences between measurements and computations are observed. These discrepancies are attributed mainly to the fact that the spatial resolution may not have been sufficient in the downslope region because in this region waves with smaller wavelengths become dominant (see Figure 4) and consequently the initially adopted resolution becomes relatively coarse.

Figures 5a-5d and Figure 6 show similar comparisons for the short monochromatic waves. The wave form in this case (short waves) does not evolve appreciably. The wave is closer to being a higher order Stokes type wave and does not behave as a shallow-water wave. Consequently, even in the shallowest region, the near resonant conditions for three-wave interactions are not satisfied and the growth rate of higher harmonics remains low.

The agreement between computations and observations for the short-wave case is not as good as that for the long waves. The reasons for this are believed to be as follows. First, the effect of wave energy dissipation is not taken into account in the numerical model. The error due to this is expected to increase with frequency, therefore should be more significant for the 0.8-Hz waves than it is for the 0.5-Hz waves. A second reason is related to the spatial resolution of the computation. The adopted relative resolution for the 0.8-Hz waves is less than for the 0.5-Hz waves, and may not have been sufficient, especially for the higher harmonics.

For the random incident waves, comparisons are given only for the "long" waves (f = 0.5 Hz) at the odd-numbered stations. The results are shown in Figure 7 (time records) and Figure 8 (spectra). (The surface elevations in Figure 7 have been normalized with H_p, the target value of $H_{1/3}$.) The spectral evolution is substantial and so is the amount of high frequency energy generation.

For the shorter waves (results not shown here), a negligible amount of high frequency energy generation was observed. The spectral shape was found to remain nearly intact at all stations.

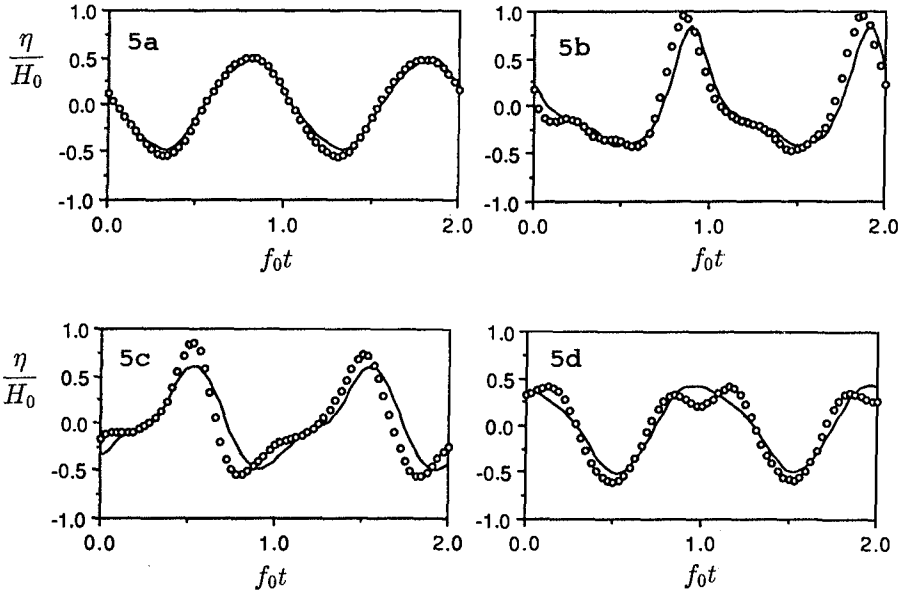

Figure 5. Measured (—) and computed (ooo) wave profiles for monochromatic waves, f=0.8 Hz, at stations 1,3,5,7 (a,b,c,d)

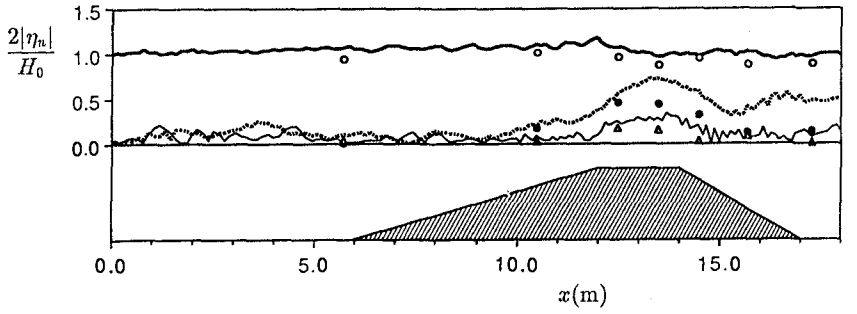

Figure 6. Measured (o: n=1)(•: n=2)(Δ: n=3) and computed (▬: n=1)(„„: n=2)(—: n=3) spatial evolution of harmonic amplitudes for monochromatic waves, f=0.8 Hz.

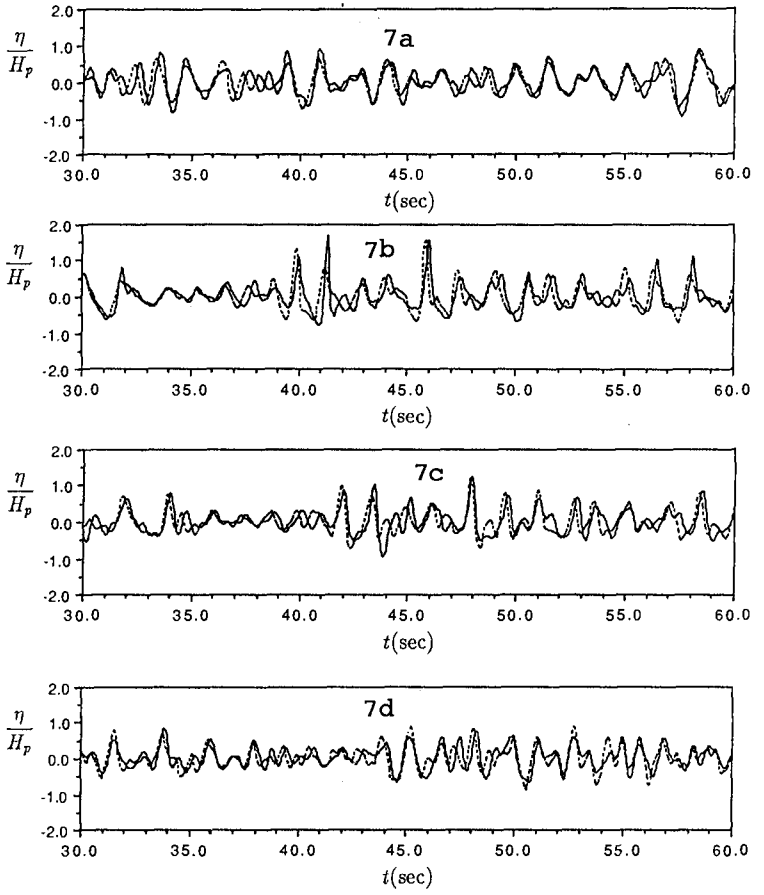

Figure 7. Measured (—) and computed (---) surface elevations for random waves, f=0.5 Hz, at stations 1,3,5,7 (a,b,c,d,)

Although the overall evolution of the random wave forms and energy spectra are well predicted by the numerical model, detailed inspection of the time domain records shows significant differences in amplitude and phases, even in the constant-depth region between wave generator and slope. These are ascribed to insufficient resolution; the normalized mesh size $\Delta x/L$ was set to 1/15 in the initial propagation domain. This may not have been sufficient to reproduce the propagation of the higher-frequency components in the (incident) waves.

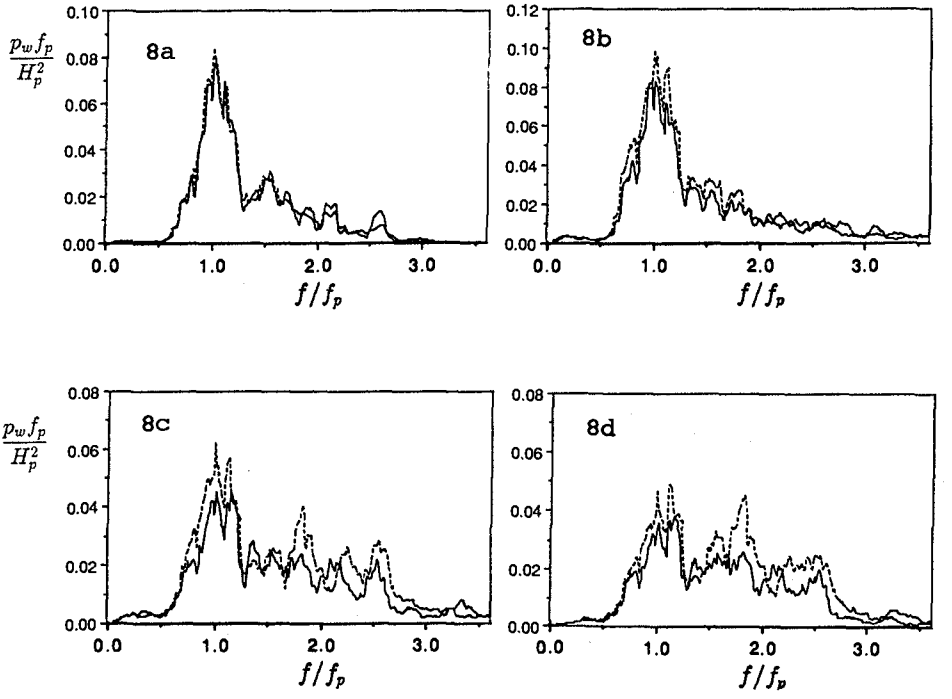

Figure 8. Measured (—) and computed (---) energy density spectra of random waves, f=0.5 Hz, at stations 1,3,5,7 (a,b,c,d)

It may further be noticed that the observed energy levels are overestimated in the computations (see e.g. the spectra at station 5 and 7 in Figure 8);the differences increase with propagation distance. This is ascribed to viscous dissipation, which is absent in the computations.

5. Conclusions

General agreement between the measurements and the computations is quite satisfactory, provided the computations are done with sufficient resolution. For the long waves the numerical model performs very well, the discrepancies are usually small. The performance of the model is less for the short waves, but still acceptable.

The comparisons presented here show some discrepancies due the absence of dissipation in the

computational model, but that is not considered a serious shortcoming for the intended applications, i.e. near-field computation of strongly non-uniform and steep wave fields near localised topographical features. In such cases, the dissipation plays a minor role, particularly at full-scale (high Reynolds number) instead of the small-scale laboratory situation of the observations discussed here.

Summarising, the results presented here confirm the reliability of the numerical model. As the cost of computing becomes lower, numerical models such as the one tested here will find wider use in engineering applications.

References

Beji, S. and J.A. Battjes, 1992. An experimental investigation of breaking and nearly breaking waves traveling over a bar. To be published in Coastal Engineering.

Dold, J.W. and D.H. Peregrine, 1984. Steep unsteady waves: an efficient computational scheme. Proc. 19th Internat. Conf. Coastal Eng. A.S.C.E. Houston 1, 955-967.

Kojima, H., T. Ijima, and A. Yoshida, 1990. Decomposition and interception of long waves by a submerged horizontal plate. Proc. 22th Coastal Eng. Con., Delft, The Netherlands, 2:1228-1241.

Longuet-Higgins, M.S. and E.D. Cokelet, 1976. The deformation of steep surface waves on water; 1. A numerical method of computation. Proc. Roy. Soc. Lond. A 350, 1-26.

Ohyama, T and K. Nadaoka, 1991. Developement of numerical wave tank for analyses of nonlinear and irregular wave field. Fluid Dynamics Res., 8:231-251.

Ohyama, T., S. Beji, K. Nadaoka and J.A. Battjes, 1992. Experimental verification of a numerical model for non-linear waves. Submitted for publication.

Phillips, O.M., 1960. On the dynamics of unsteady gravity waves of finite amplitude, Part 1. The elementary interactions, J. Fluid Mech., 9:193-217.

Vinjé, T, and P. Brevig, 1981. Numerical simulation of breaking waves. Adv. Water Resources 4, 77-82.